ARTICLES
PUBLISHED ONLINE: 18 APRIL 2016 | DOI: 10.1038/NCHEM.2492
nature chemistry

A highly stretchable autonomous self-healing elastomer

Cheng-Hui Li[1,2†], Chao Wang[1,3†], Christoph Keplinger[4,5,6], Jing-Lin Zuo[2], Lihua Jin[7], Yang Sun[8], Peng Zheng[2], Yi Cao[8], Franziska Lissel[1], Christian Linder[7], Xiao-Zeng You[2] and Zhenan Bao[1*]

It is a challenge to synthesize materials that possess the properties of biological muscles—strong, elastic and capable of self-healing. Herein we report a network of poly(dimethylsiloxane) polymer chains crosslinked by coordination complexes that combines high stretchability, high dielectric strength, autonomous self-healing and mechanical actuation. The healing process can take place at a temperature as low as −20 °C and is not significantly affected by surface ageing and moisture. The crosslinking complexes used consist of 2,6-pyridinedicarboxamide ligands that coordinate to Fe(III) centres through three different interactions: a strong pyridyl–iron one, and two weaker carboxamido–iron ones through both the nitrogen and oxygen atoms of the carboxamide groups. As a result, the iron–ligand bonds can readily break and re-form while the iron centres still remain attached to the ligands through the stronger interaction with the pyridyl ring, which enables reversible unfolding and refolding of the chains. We hypothesize that this behaviour supports the high stretchability and self-healing capability of the material.

Animal muscle is a biomaterial that has long fascinated the scientific world: it is strong, elastic and able to undergo self-healing when wounded. Synthetic polymers have been designed to self-heal by encapsulating healing agents or incorporating dynamic bonds[1–3]. However, most of these approaches require the input of energy (either heat or light)[4–6] or the assistance of a liquid monomer and catalyst[7], solvents[8] or plasticizers[9]. Of the few examples of autonomous self-healing rubbers, most are based on moisture-sensitive hydrogen bonding[10–15], and therefore lack stability against moisture.

We describe herein a design concept that takes advantage of the versatility in tuning the strength of metal–ligand interactions to achieve high strength, high stretchability and room-temperature self-healing that is not significantly affected by surface ageing (which occurs when a surface is exposed to air for some time without protection). Previous work that involved metal–ligand interactions for self-healing materials either relied on strong bonds, which required an external stimulus for healing[4,16–20], or weak bonds, which could not provide sufficient mechanical strength[21,22]. To combine autonomous and reversible healing at room temperature, a weak bonding strength is generally required together with a low glass-transition temperature (T_g) to enable polymer mobility.

Here we placed strong metal–ligand binding sites adjacent to weak binding sites in a single ligand, 2,6-pyridinedicarboxamide, which resulted in highly dynamic metal–ligand interactions. The weaker bonds can readily break and re-form, which is favourable for energy dissipation on stretching and self-healing on being damaged, with the metal ions still maintained near the ligands by the stronger interactions, which allows a rapid bond re-formation. We observed that the cooperative effect of these binding sites enables simultaneously very high stretchability and autonomous self-healing with good mechanical and dielectric strength. Furthermore, we demonstrate the material's application towards self-healing artificial muscle actuators.

Results and discussions

Material design and characterizations. We selected an Fe(III)-2,6-pyridinedicarboxamide (pdca) coordination complex for our design. To understand the coordination complex formed in the polymer networks, we prepared a model ligand, 2,6-butylpyridinedicarboxamide (H_2Bupdca (Supplementary Fig. 1)), and used mass spectrometry to characterize the complex formed under similar conditions to those used to prepare the polymer networks (see the Supplementary Information for details). The measured molecular mass corresponded well with the mass of $[Fe(HBupdca)_2]^+$, as shown in Supplementary Fig. 2a, which suggests that in the most-stable complex formed only one of the two amide groups was deprotonated on reacting with $FeCl_3$ without the addition of a base. This structure was characterized further and confirmed by ultraviolet–visible (UV-vis) and Fourier transform infrared (FTIR) spectra, as well as by density functional theory (DFT) calculations (Supplementary Figs 3–5).

The bonding energies of Fe(III)–$N_{pyridyl}$, Fe(III)–N_{amido} and Fe(III)–O_{amido} bonds were further estimated as 145.0, 82.7 and 40.7 kcal mol^{-1}, respectively, based on calculations with bond-valence–bond-length correlations (Supplementary Table 1). The stronger Fe(III)–$N_{pyridyl}$ bond is comparable to typical covalent bonds, which can be used to enhance the modulus of the material, whereas the weaker Fe(III)–O_{amido} bond is almost as weak as

[1]Department of Chemical Engineering, Stanford University, Stanford, California 94305, USA. [2]State Key Laboratory of Coordination Chemistry, School of Chemistry and Chemical Engineering, Collaborative Innovation Center of Advanced Microstructures, Nanjing University, Nanjing 210093, China. [3]Department of Chemistry, University of California Riverside, Riverside, California 92521, USA. [4]Department of Chemistry and Chemical Biology, Harvard University, Cambridge, Massachusetts 02138, USA. [5]Department of Mechanical Engineering, University of Colorado, Boulder, Colorado 80309, USA. [6]Materials Science and Engineering Program, University of Colorado, Boulder, Colorado 80309, USA. [7]Department of Civil and Environmental Engineering, Stanford University, Stanford, California 94305, USA. [8]National Laboratory of Solid State Microstructure, Department of Physics, Collaborative Innovation Center of Advanced Microstructures, Nanjing University, Nanjing 210093, China. †These authors contributed equally to this work.
*e-mail: zbao@stanford.edu

© 2016 Macmillan Publishers Limited. All rights reserved

hydrogen bonding. Both interactions are stabilized through a chelating effect. However, once the weak bonding sites are broken, the strength of the strong bonding sites is also weakened, which makes the coordination structure more fragile. Therefore, the combination of strong and weak bonding sites in a single ligand provides both strong crosslinking and energy dissipation mechanisms for strain (Fig. 1a,b).

The Fe(III)-pdca coordination complex described above was introduced into a linear poly(dimethylsiloxane) (PDMS) polymer backbone, and served as a crosslinking unit (Fig. 1c). Briefly, the PDMS oligomer that contained 2,6-pyridinedicarboxamide (H_2pdca) groups (denoted as H_2pdca-PDMS) was prepared by condensation reactions between bis(3-aminopropyl)-terminated poly (dimethylsiloxane) (H_2N-PDMS-NH_2, M_n = 5,000–7,000) and 2,6-pyridinedicarbonyl dichloride to give a colourless viscous liquid. The H_2pdca-PDMS liquid was subsequently crosslinked into a dark-red solid by Fe(III) chloride, with a molar ratio of Fe(III) ion to H_2pdca ligand of 1:2. The UV-vis spectrum of the polymer film shows a band at 362 nm, as shown in Supplementary Figs 6 and 7, similar to the absorption wavelength observed for $[Fe(HBupdca)_2]Cl$, which indicates the dominant presence of such complexes (denoted as Fe-Hpdca-PDMS). Furthermore, the intensity of N–H stretching at 3,315 and 3,335 cm^{-1} partially decreased and a red shift of the amide C=O stretching frequency was observed in the FTIR spectra (Supplementary Fig. 8). Raman studies indicate that both Fe–N and Fe–O coordination bonds are present in the as-prepared polymer. The percentage of Fe–O coordination increased with the molar ratio of Fe(III) ion to H_2pdca ligand (Supplementary Fig. 9). In association with the long wavelength tail at $\lambda > 400$ nm in the UV-vis spectrum, the resulting polymer network probably contains a mixture of various coordination structures. The tail above 400 nm is more significant in thick films, and we suggest this arises from the presence of low-energy absorbing Fe(III) complexes (Supplementary Fig. 7).

Both intrachain and interchain complexations are expected to occur in the Fe-Hpdca-PDMS polymer matrix (Fig. 1c). The intrachain ones will result in folding of the PDMS chain, whereas the interchain ones will give rise to three-dimensional (3D) crosslinking. We used single-molecule force spectroscopy to characterize the presence of those bonding features. Two single polymer chains of H_2pdca-PDMS and Fe-Hpdca-PDMS, respectively, were first stretched to an extended state. Stretching of H_2pdca-PDMS results in only one force peak (Fig. 1d), which corresponds to the detachment of the macromolecule from the substrate. However, stretching of Fe-Hpdca-PDMS leads to typical sawtooth-like force–extension curves (Fig. 1d), in which the different force peaks correspond to the unfolding of PDMS units through the rupture of coordination bonds in the $[Fe(Hpdca)_2]^+$ complexes. The contour length increments (that is, the increased lengths caused by the unfolding of the polymer chain), defined as ΔL_c, are about 12 ± 2 nm or $(12 \pm 2)n$ nm (n = 1–5) and correspond well to one or multiple molecular lengths of NH_2-PDMS-NH_2 with an M_n of 5,000–7,000 (Supplementary Fig. 10). According to the statistics data of the experiment, the rupture force of the $Fe[(Hpdca)_2]^+$ coordination complexes was about 103 ± 12 pN (Supplementary Fig. 11).

To investigate whether the unfolding and stretching of Fe-Hpdca-PDMS is reversible, we released the unfolded Fe-Hpdca-PDMS chain to zero force. After waiting for one second, we stretched the Fe-Hpdca-PDMS chain again to probe whether it could fold back to its original state. As shown in Fig. 1e, we observed the reversible unfolding/refolding of Fe-Hpdca-PDMS. These features are similar to those observed in the iron–sulfur protein rubredoxin in which single-molecule force spectroscopy also revealed characteristic sawtooth features on single-chain extension[23,24]. These features were attributed to the ferric ion still being attached to cysteine loops and able to refold quickly to reconstitute the iron–cysteine centre. In our case, the single chain of the Fe-Hpdca-PDMS molecule was elongated on stretching accompanied by rupture of the $[Fe(Hpdca)_2]^+$ coordination complex, whereas the iron remained bound to one $Hpdca^-$ motif, which resulted in a metastable $[Fe(Hpdca)]^{2+}$ intermediate. The macromolecule can then collapse on releasing the strain, and the other $Hpdca^-$ can chelate again to $[Fe(Hpdca)]^{2+}$ to re-form an $[Fe(Hpdca)_2]^+$ centre, which initiates the complete refolding of Fe-Hpdca-PDMS. Therefore, the single-chain Fe-Hpdca-PDMS molecule can be unfolded and refolded because of the rupture and reconstruction of $[Fe(Hpdca)_2]^+$ complexes (Fig. 1e and Supplementary Fig. 12).

Rheological and mechanical properties. The T_g for the resulting polymer network was measured to be below −90 °C (Supplementary Figs 13 and 14), which is typical for silicone rubbers. Rheological measurements at room temperature showed that its storage modulus, G', is comparable to the loss modulus, G'', at low frequencies. However, G' increased faster with increasing frequency than did G'' (Supplementary Fig. 15a). Such features are characteristic for typical crosslinked polymer networks and for soft glassy materials[25]. On increasing the temperature, both G' and G'' decreased, but G' decreased more rapidly than G'' (Supplementary Fig. 15b), which suggests that the polymer becomes more viscous and fluid-like at higher temperatures and thus potentially facilitates the self-healing.

The obtained Fe-Hpdca-PDMS polymer exhibited good mechanical strength and very high stretchability (Fig. 2). The Young's modulus of the polymer film is calculated to be 0.54 ± 0.1 MPa from the low-strain region (<20% strain) of the stress–strain curve (Supplementary Table 2), which indicates the high binding strength of the metal–ligand interaction. The stress–strain curves consist of an initial stiffening region (in which the tension significantly increases with the increase of the strain), followed by a subsequent steady region in which the stress is almost constant on further increases in strain until the polymer film breaks apart. Cyclic stress–strain tests with a maximum applied strain of 1,500% showed pronounced hysteresis, which indicates energy dissipation from bond breakage. There is always a pronounced hysteresis in cyclic stress–strain tests, even when the sample is subjected to only a 30% strain (Supplementary Fig. 16). However, if the same polymer film was stretched and released successively, the tensional stresses of the second stretch would be significantly lower than those of the previous cycle. The same polymer film was then allowed to rest for one hour, and stretched again. It showed an almost fully self-recovery—that is, a very similar behaviour to that of the original stress–strain behaviours (Fig. 2d). When the polymer films were stretched and maintained under strain for one hour, they needed a longer time to recover and did not fully return to their original state (we observed only partial recovery even after resting for one day). These observations are similar to those of previously reported hydrogen-boned crosslinked elastomers and hydrogels based on ionic crosslinking[26,27]. In such materials, the non-covalent bonds break and dissipate the strain energy; after release of the mechanical strain, the broken bonds can be partially recovered to restore most of the mechanical properties.

Fe-Hpdca-PDMS can be stretched to a much higher strain before fracturing than can typical crosslinked PDMS or other reported supramolecular elastomers (Fig. 2c and Supplementary Fig. 17). A maximum fracture strain up to $4,500 \pm 20\%$ can be achieved for a sample of 1 mm thickness, 2 mm gauge length and 6 mm width at a loading rate of 2 mm min^{-1}. The sample can self-recover to its original length within one hour of release of the stress (release immediately after strain). When we decreased the amount of metal ions, at a molar ratio of Fe(III) to H_2pdca-PDMS of 1:6, the polymer showed irreversible deformation. With this ratio, the material can even be stretched to over 100 times its original

© 2016 Macmillan Publishers Limited. All rights reserved

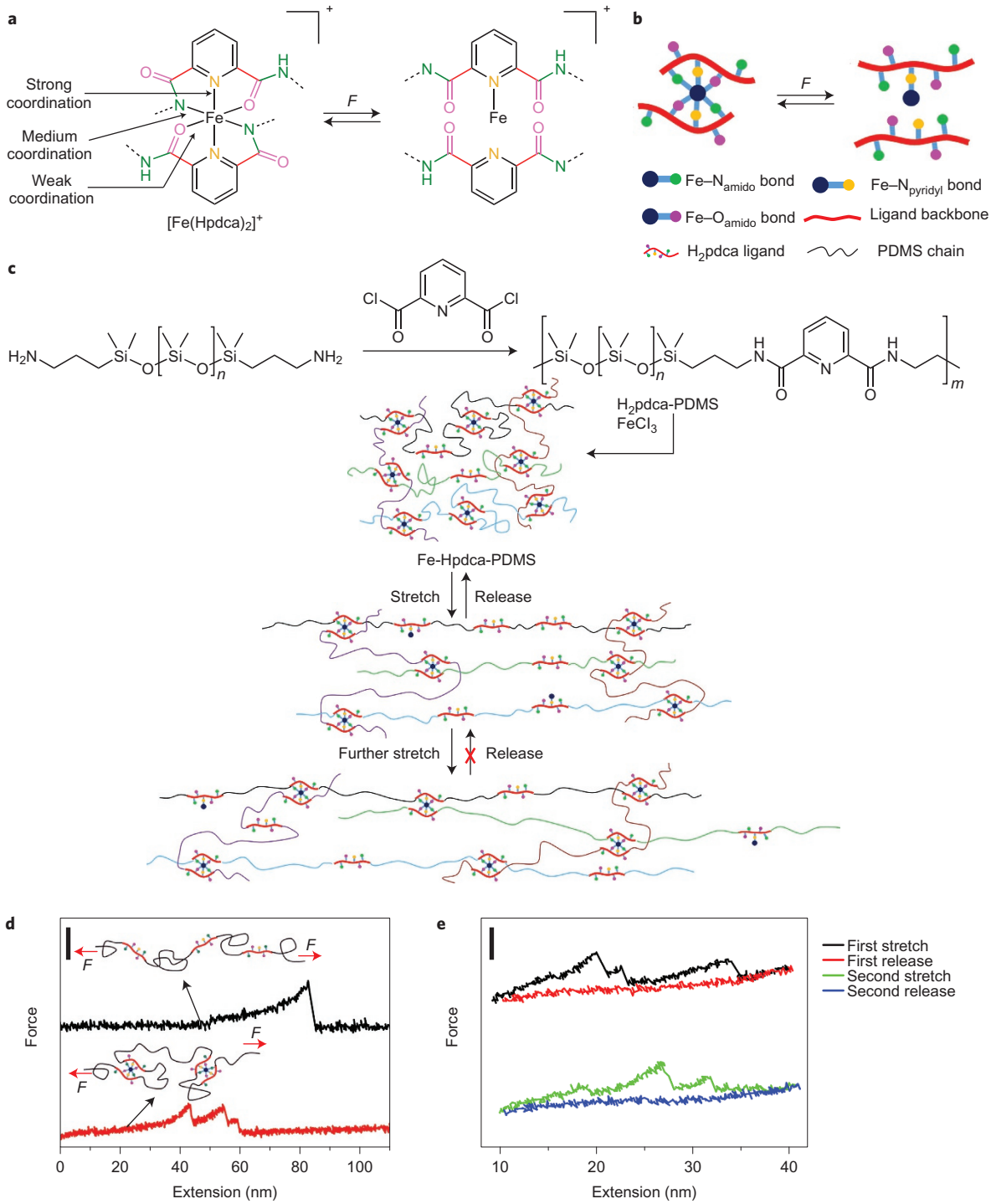


Figure 1 | Schematic structure of material design and single-molecule force spectroscopy characterization. a,**b**, Structure (**a**) and schematic illustration (**b**) xof the $[Fe(Hpdca)_2]^+$ moiety undergoing reversible rupture and reconstruction during tensile stretching (using a force *F*) of the films. Note, key refers to entire figure. **c**, Synthesis and structure of the material, and proposed mechanism for chain folding and sliding during tensile stretching. PDMS chains shown in different colours represent different polymers. **d**, Typical force–extension curves during force spectroscopy measurements of the stretching of a single chain of H_2pdca-PDMS and of Fe-Hpdca-PDMS. For H_2pdca-PDMS the curve shows only one step, which corresponds to detachment from the substrate, whereas for Fe-Hpdca-PDMS several peaks are observed for the rupture of the $[Fe(Hpdca)_2]^+$ centres during stretching. Scale bar for the vertical axis, 150 pN. **e**, Typical force–extension curves of Fe-Hpdca-PDMS from stretching–releasing cycles that show reversible unfolding and refolding. Scale bar for the vertical axis, 150 pN.

length without breaking, and can partially recover after resting for 12 hours (Fig. 2a,b and Supplementary Fig. 18). In comparison, typical covalent-crosslinked PDMS rubbers with similar dimensions exhibit a maximum elongation of only 100–1,100% (ref. 28). To the best of our knowledge, the most stretchable hydrogen-bonded polymers reported so far exhibit a reversible stretchability at about 2,000% strain[26].

We propose that the high stretchability of the Fe-Hpdca-PDMS material can be attributed to the unique bonding features in an Fe-Hpdca complex. Both intrachain and interchain metal–ligand

© 2016 Macmillan Publishers Limited. All rights reserved

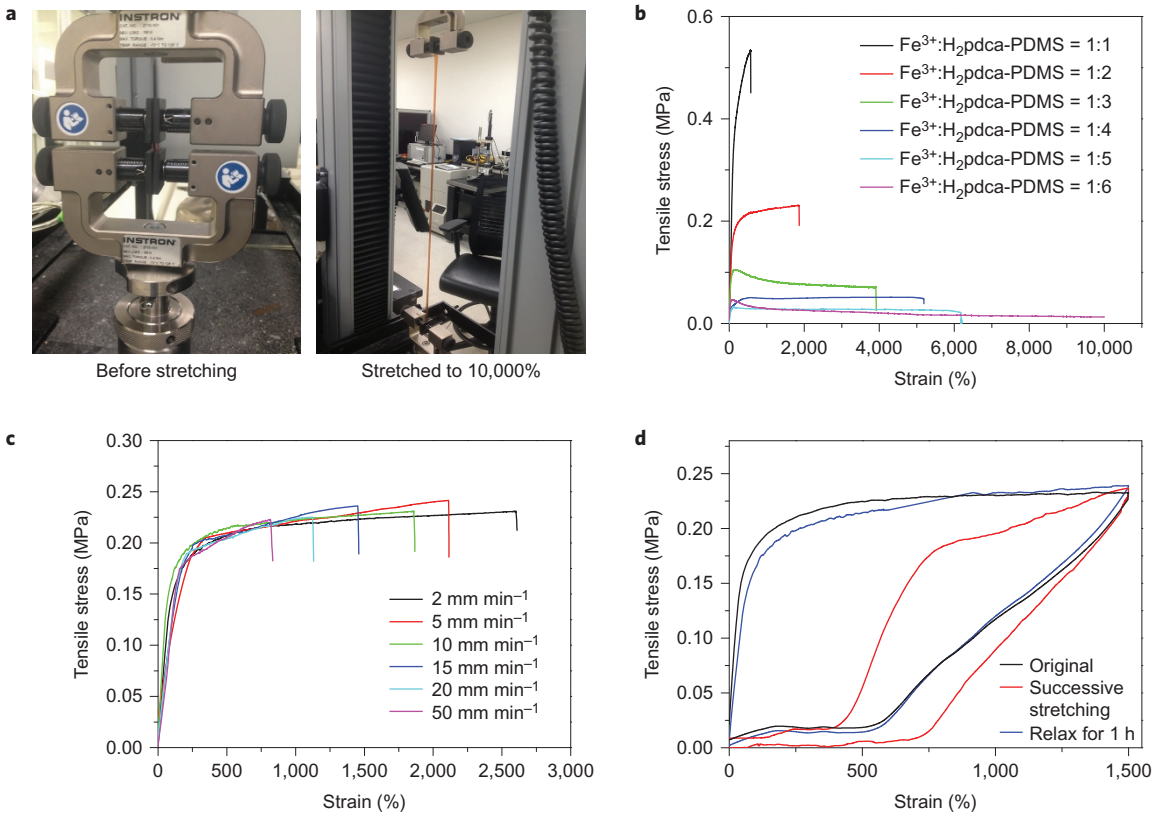


Figure 2 | Mechanical properties of Fe-Hpdca-PDMS. a, Photographs of a film (with an Fe(III) metal to H_2pdca-PDMS ligand molar ratio of 1:6) before and after stretching. **b**, Tensile stress curves of films prepared with different molar ratios of Fe(III) metal to H_2pdca-PDMS ligand show that decreasing the number of Fe centres makes the films more stretchable. **c**, Stress–strain curve of the film prepared with an Fe(III) metal to H_2pdca-PDMS ligand molar ratio of 1:2 stretched at different speeds for a sample of width 14 mm, thickness 1 mm and gauge length 2 mm. **d**, Stress–strain curve of the film prepared with an Fe(III) metal to H_2pdca-PDMS ligand molar ratio of 1:2 in cyclic stress–strain tests (up to 1,500% strain) as prepared (black), stretched immediately after the first release process (red), then allowed to rest for one hour after release of the strain and stretched again (blue), with a sample width of 14 mm, thickness of 1 mm, gauge length of 2 mm and loading rate of 10 mm min^{-1}.

interactions are present in the Fe-Hpdca-PDMS polymer. The intra-chain metal–ligand interaction results in folding of the PDMS chain, which allows a large chain extension on breakage, whereas the inter-chain metal–ligand interaction leads to 3D crosslinking and potentially repeated bonding/breakage between chains through chain sliding. The dynamic nature of Fe–Hpdca bonds allows them to break and re-form during stretching, which leads to the unfolding and sliding of the polymer chains and renders the high stretchability of the material. Therefore, this material offers multiple mechanisms for energy dissipation, which makes the material tough (fracture energy ~2,571 ± 20 J m^{-2} (Supplementary Fig. 19)). Additionally, compared with hydrogen bonds, which can only dissipate the strain energy by bond breakage, the Fe-Hpdca complex can offer multiple modes of bond breaking, exchanging and re-formation: (1) bond breakage of the weaker carboxamido–Fe(III) sites as the stronger pyridyl–Fe(III) bonds hold them in close proximity[14,29–31] and (2) dynamic rupture and reconstruction of the carboxamido–Fe(III) bonding configurations during chain unfolding and sliding. Unlike the highly directional hydrogen bonds, our Fe–Hpdca bonds are diverging, so that the breakage, re-formation and exchange of the bonds can take place more readily. Such reversible bond breakage and recovery has been observed previously by Craig and co-workers for a PDMS system that incorporates mechanoresponsive bonds[32].

Our proposed carboxamido–Fe(III) bond re-formation/switching mechanism is also supported by experimental observations. First, the stretchability of the films is strongly dependent on the stretching speed (Fig. 2c). As the strain speed increases, less time is allowed for the re-formation of the broken Fe(III)–amide bonds, which reduces the fracture tolerance. Second, when we used PDMS of different molecular weight (M_n = 2,500–4,000 or 15,000–20,000) as starting materials, the stretchability of the polymer decreased (Supplementary Fig. 20). A starting polymer with a PDMS of higher molecular weight has fewer metal-coordination binding sites for bond reconstruction through chain sliding. A starting polymer with a PDMS of lower molecular weight has more metal-coordination binding sites, as evidenced by the increase of stress, but it shows poorer stretchability because of the shorter PDMS chain with a limited folding/unfolding ability.

Self-healing properties. Our Fe-Hpdca-PDMS polymer not only has a high stretchability, but also exhibits a self-healing capability at room temperature. To demonstrate the self-healing capability, the polymer film was cut into two pieces and subsequently put together to allow healing under different conditions (Supplementary Figs 21–23). The cut on the polymer film was observed to almost disappear after healing at room temperature for 48 hours, although minor scars were still visible (Fig. 3a). To make the cut region more distinguishable, one of the two pieces was stained using a black dye. As shown in Fig. 3b, the healed polymer film can again sustain a large strain after a healing duration of 48 hours at room temperature. As expected, a longer healing time and higher healing temperature both resulted in a higher recovered fracture strain (Fig. 3c and Supplementary Fig. 22). Healing at room temperature for 48 hours led to a recovered fracture strain of 1,700 ± 60% and a high healing efficiency (η) of 90 ± 3% (Fig. 3c). The healing even

© 2016 Macmillan Publishers Limited. All rights reserved

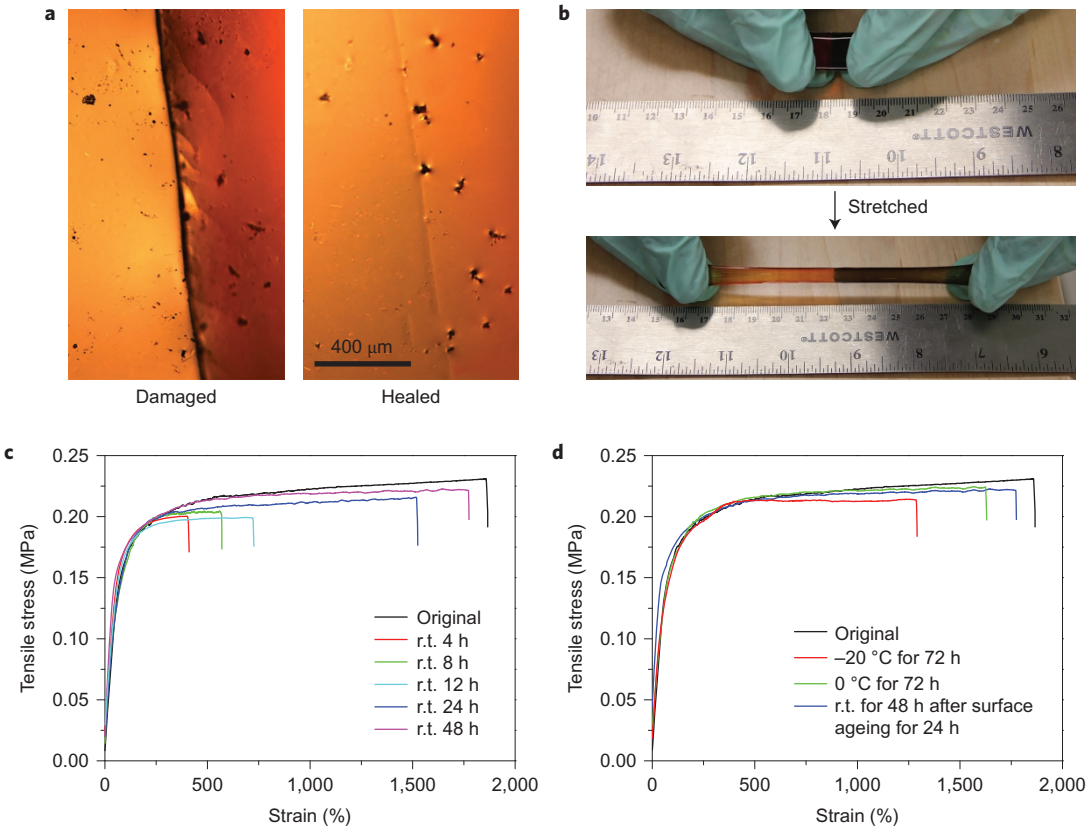


Figure 3 | Self-healing properties of the Fe-Hpdca-PDMS film (with an Fe(III) metal to H_2pdca-PDMS ligand molar ratio of 1:2. a, Optical microscope images of damaged and healed samples. **b**, Optical images of the healed film before and after stretching. **c**, Stress–strain curves of a film healed at room temperature (r.t.) for different lengths of time show an increase of the stretching ability when the film is allowed to heal for longer. **d**, The stress–strain curves of the film healed at –20 and 0 °C for 72 hours, and the stress–strain curves of the film healed at room temperature for 48 hours after surface ageing for 24 hours. The measuring conditions for the tensile test were a width of 14 mm, thickness of 1 mm, gauge length of 2 mm and loading rate of 10 mm min^{-1}.

took place at –20 °C to give a healing efficiency of 68 ± 2% after 72 hours (Fig. 3d). To the best of our knowledge, this is the first report of autonomous self-healing at such a low temperature without the addition of any stimulus.

As a comparison, two undamaged polymer films can also be joined together through self-healing. We cut a polymer film into two pieces and placed these in contact with each other through undamaged surfaces (Supplementary Fig. 24a). After healing at room temperature for 48 hours, the rejoined polymer film can sustain a 1,060 ± 30% strain with a healing efficiency of 57 ± 2% (Supplementary Fig. 24b), in contrast with a healing efficiency of 90 ± 2% for the cut-surface healing under similar conditions (Fig. 3c). The lower healing efficiency is because fewer reactive sites are available without both cutting and a rough surface at the healing site, and this results in insufficient molecular diffusion. Nevertheless, this suggests the existence of a dynamic exchange of metal–ligand coordination bonds in the polymer matrix.

Unlike self-healing materials based on hydrogen bonding[10–15], the self-healing of the Fe-Hpdca-PDMS polymer is not significantly affected by surface ageing. On cutting the polymer film into two separate pieces, separated at ambient temperature for 24 hours and then healed at room temperature for 48 hours, we observed that the healing efficiency still reached 90 ± 3%, a value similar to the healing efficiency of freshly cut and healed pieces (Fig. 3d). The cycle of stretching, breaking and healing can be repeated multiple times. The excellent self-healing properties of Fe-Hpdca-PDMS are attributed to two factors: (1) the presence of abundant dynamic metal–ligand coordination bonds, similar to other self-healing polymers[1–4,16–20,33–38], and (2) the low T_g (below –90 °C) of the polymer gives a high mobility to the polymer chains, which enables self-healing, even at a low temperature.

Application in artificial muscles. In addition to the high stretchability and low-temperature self-healing, the Fe-Hpdca-PDMS polymer with an Fe(III) metal to H_2pdca-PDMS ligand molar ratio of 1:2 has a high dielectric constant (6.4 ± 0.1) (Supplementary Fig. 25) and dielectric strength (a preliminary unoptimized result gave 18.8 ± 0.5 MV m^{-1}). Moreover, the deformation of the Fe-Hpdca-PDMS polymer film on stretching at low strain is quite fast and has a small hysteresis (Supplementary Fig. 16), which are desirable properties for investigations in artificial muscles[39–45]. Figure 4 shows a pristine elastomer film of Fe-Hpdca-PDMS with a thickness of 640 μm being punctured by a sharp-pointed object (Fig. 4b). The sample was subsequently stored for 72 hours at room temperature. A square-wave high-voltage signal (1 Hz, 11 kV maximum voltage, 0 kV minimum voltage) was then applied through the coated carbon electrodes over the healed region, which caused the dielectric elastomer actuator to deform visibly (see Supplementary Movie 1). Figure 4e,f shows still images of the actuator at 0 kV (0 MV m^{-1}) and 11 kV (>17.2 MV m^{-1}), respectively. The high applied electric field caused an area expansion of 3.6% in the elastomer; however, it did not cause any electric breakdown at the location of the mechanical damage. The ability to withstand electric fields above 17 MV m^{-1} after self-healing indicates the excellent self-healing ability of the material. On increasing the maximum voltage of the square-wave signal to 12 kV (>18.8 MV m^{-1}), we observed the electric breakdown of the sample (Supplementary Movie 2). Despite the inflicted damage, the self-healed film still retained values

© 2016 Macmillan Publishers Limited. All rights reserved

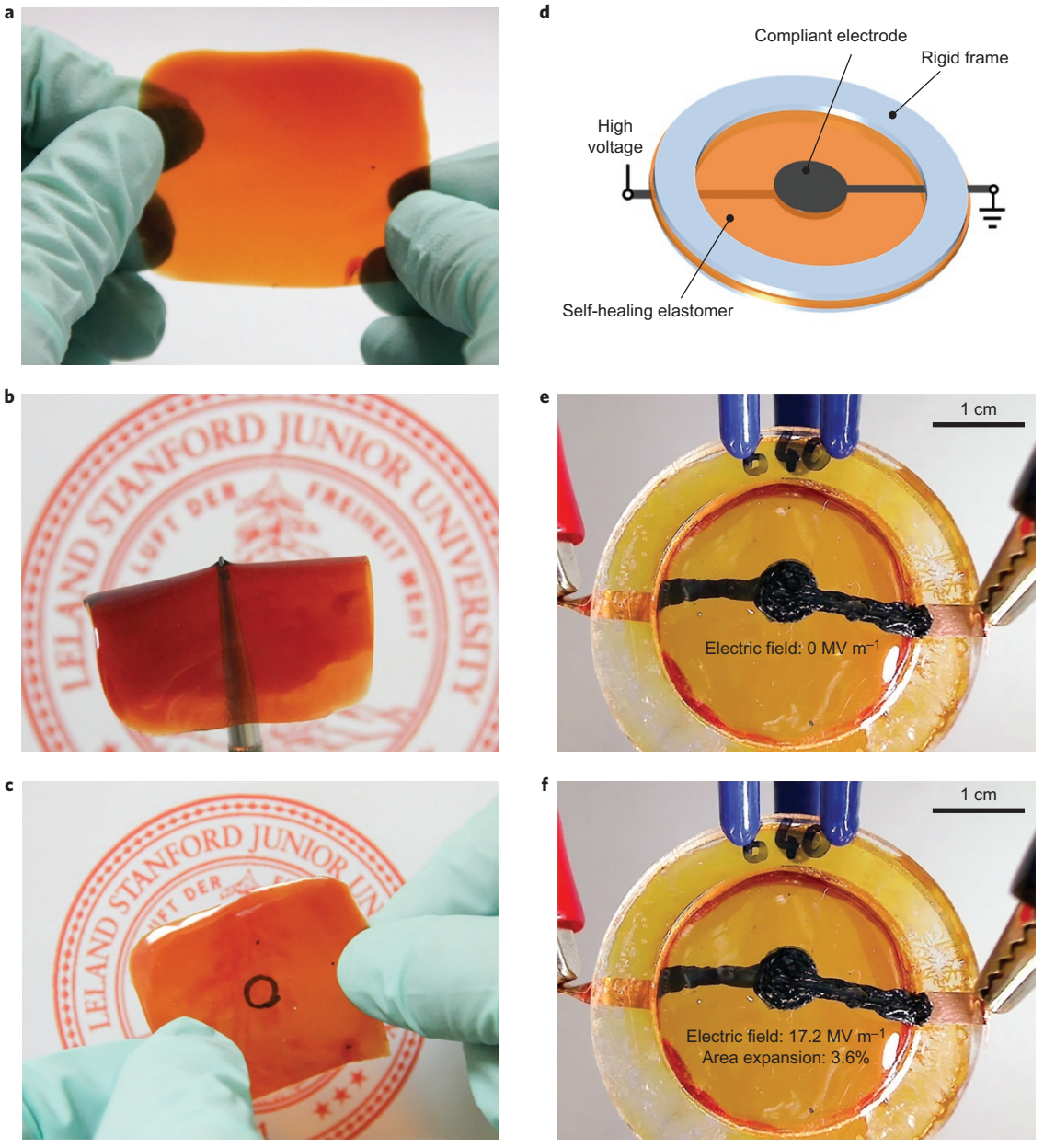


Figure 4 | Self-healing artificial muscle fabricated from a Fe-Hpdca-PDMS film with an Fe(III) metal to H_2pdca-PDMS ligand molar ratio of 1:2. a, Pristine film of the self-healing elastomer. **b**, A pointed object that penetrated the film caused severe mechanical damage. **c**, Condition of the sample after 72 hours of healing at room temperature. The location of the former mechanical damage is marked with a circle. **d**, Experimental set-up to assess the aptitude of the healed sample for use in a dielectric elastomer actuator. Two circular rigid frames held the elastomeric film in place. The location of the previous mechanical damage was sandwiched between compliant electrodes, a high electric field was applied across the thickness of the elastomer and caused the area sandwiched by the electrodes to expand. **e**,**f**, Photos of the dielectric elastomer actuator before (**e**) and after (**f**) the application of a high voltage. The high electric field induced an area expansion of 3.6%, but it did not cause a dielectric breakdown at the location of the self-healing event.

comparable to those of the pristine polymer. The present Fe-Hpdca-PDMS elastomer is highly tunable by varying the ligand-to-metal molar ratio and adding functional groups to the ligand and so potentially can be further optimized for specific requirements of an actuator, which will be the subject of future studies.

Conclusions

In summary, we have developed a highly stretchable and autonomous self-healing material by incorporating coordination complexes with various bond strengths as crosslinks between the polymer chains. The dynamic nature of the metal–ligand bond allows it to be broken and re-formed during stretching, which leads to unfolding and sliding of the polymer chains and so renders the high stretchability of the material. The as-prepared material can be stretched to 45 ± 2 times its original length and recovered on releasing the strain. Even in the absence of any additives to promote the healing process, such as plasticizers or solvents, or of external energy, the film displays excellent self-healing properties down to a low temperature of −20 °C. We believe that the material's ability to restore a high dielectric strength after recovery from mechanical damage makes it promising for artificial muscle applications, and envisage that the design concepts presented here may represent a general approach to the preparation of highly stretchable functional materials.

Received 8 October 2015; accepted 3 March 2016;
published online 18 April 2016

© 2016 Macmillan Publishers Limited. All rights reserved

References

1. Wu, D. Y., Meure, S. & Solomon, D. Self-healing polymeric materials: a review of recent developments. *Prog. Polym. Sci.* **33,** 479–522 (2008).
2. Yang, Y. & Urban, M. W. Self-healing polymeric materials. *Chem. Soc. Rev.* **42,** 7446–7467 (2013).
3. Binder, W. H. *Self-Healing Polymers: From Principles to Applications* (Wiley-VCH, 2013).
4. Burnworth, M. *et al.* Optically healable supramolecular polymers. *Nature* **472,** 334–337 (2011).
5. Ghosh, B. & Urban, M. W. Self-repairing oxetane-substituted chitosan polyurethane networks. *Science* **323,** 1458–1460 (2009).
6. Chen, X. *et al.* A thermally re-mendable cross-linked polymeric material. *Science* **295,** 1698–1702 (2002).
7. Toohey, K. S., Sottos, N. R., Lewis, J. A., Moore, J. S. & White, S. R. Self-healing materials with microvascular networks. *Nature Mater.* **6,** 581–585 (2007).
8. Caruso, M. M. *et al.* Solvent-promoted self-healing epoxy materials. *Macromolecules* **40,** 8830–8832 (2007).
9. Jackson, A. C., Bartelt, J. A. & Braun, P. V. Transparent self-healing polymers based on encapsulated plasticizers in a thermoplastic matrix. *Adv. Funct. Mater.* **21,** 4705–4711 (2011).
10. White, S. R. *et al.* Autonomic healing of polymer composites. *Nature* **409,** 794–797 (2001).
11. Wang, Q. *et al.* High-water-content mouldable hydrogels by mixing clay and a dendritic molecular binder. *Nature* **463,** 339–343 (2010).
12. Cordier, P., Tournilhac, F., Soulie-Ziakovic, C. & Leibler, L. Self-healing and thermoreversible rubber from supramolecular assembly. *Nature* **451,** 977–980 (2008).
13. Tee, B. C.-K., Wang, C., Allen, R. & Bao, Z. An electrically and mechanically self-healing composite with pressure- and flexion-sensitive properties for electronic skin applications. *Nature Nanotech.* **7,** 825–832 (2012).
14. Chen, Y., Kushner, A. M., Williams, G. A. & Guan, Z. Multiphase design of autonomic self-healing thermoplastic elastomers. *Nature Chem.* **4,** 467–472 (2012).
15. Wang, C. *et al.* A rapid and efficient self-healing thermo-reversible elastomer crosslinked with graphene oxide. *Adv. Mater.* **25,** 5785–5790 (2013).
16. Balkenende, D. W. R. *et al.* Mechanochemistry with metallosupramolecular polymers. *J. Am. Chem. Soc.* **136,** 10493–10498 (2014).
17. Bode, S. *et al.* Self-healing polymer coatings based on crosslinked metallosupramolecular copolymers. *Adv. Mater.* **25,** 1634–1638 (2013).
18. Bode, S. *et al.* Self-healing metallopolymers based on cadmium bis(terpyridine) complex containing polymer networks. *Polym. Chem.* **4,** 4966–4973 (2013).
19. Sandmann, B. *et al.* The self-healing potential of triazole–pyridine-based metallopolymers. *Macromol. Rapid Commun.* **36,** 604–609 (2015).
20. Yang, B. *et al.* Self-healing metallo-supramolecular polymers from a ligand macromolecule synthesized via copper-catalyzed azide–alkyne cycloaddition and thiol–ene double 'click' reactions. *Polym. Chem.* **5,** 1945–1953 (2014).
21. Krogsgaard, M., Behrens, M. A., Pedersen, J. S. & Birkedal, H. Self-healing mussel-inspired multi-pH-responsive hydrogels. *Biomacromolecules* **14,** 297–301 (2013).
22. Basak, S., Nanda, J. & Banerjee, A. Multi-stimuli responsive self-healing metallo-hydrogels: tuning of the gel recovery property. *Chem. Commun.* **50,** 2356–2359 (2014).
23. Zheng, P., Wang, Y. & Li, H. Reversible unfolding–refolding of rubredoxin: a single-molecule force spectroscopy study. *Angew. Chem. Int. Ed.* **53,** 14060–14063 (2014).
24. Zheng, P., Arantes, G. M., Field, M. J. & Li, H. Force-induced chemical reactions on the metal centre in a single metalloprotein molecule. *Nature Commun.* **6,** 7569 (2015).
25. Sollich, P. Rheological constitutive equation for a model of soft glassy materials. *Phys. Rev. E* **58,** 738–759 (1998).
26. Sun, J. Y. *et al.* Highly stretchable and tough hydrogels. *Nature* **489,** 133–136 (2012).
27. Sun, T. L. *et al.* Physical hydrogels composed of polyampholytes demonstrate high toughness and viscoelasticity. *Nature Mater.* **12,** 932–937 (2013).
28. Bhowmick, A. K., & Stephens, H. *Handbook of Elastomers* (CRC Press, 2000).
29. Iyer, B. V. S. *et al.* Modeling the response of dual cross-linked nanoparticle networks to mechanical deformation. *Soft Matter* **9,** 109–121 (2013).
30. Iyer, B. V. S. *et al.* Strain recovery and self-healing in dual cross-linked nanoparticle networks. *Polymer Chem.* **4,** 4927–4939 (2013).
31. Iyer, B. V. *et al.* Ductility, toughness and strain recovery in self-healing dual cross-linked nanoparticle networks studied by computer simulations. *Prog. Polymer Sci.* **40,** 121–137 (2015).
32. Gossweiler, G. R. *et al.* Mechanochemical activation of covalent bonds in polymers with full and repeatable macroscopic shape recovery. *ACS Macro Lett.* **3,** 216–219 (2014).
33. Holten-Anderson, N. *et al.* pH-induced metal–ligand crosslinks inspired by mussel yield self-healing polymer networks with near covalent elastic moduli. *Proc. Natl Acad. Sci. USA* **108,** 2651 (2011).
34. Grindy, S. C. *et al.* Control of hierarchical polymer mechanics with bioinspired metal-coordination dynamics. *Nature Mater.* **14,** 1210–1216 (2015).
35. Kushner, A. M., Gabuchian, V., Johnson, E. G. & Guan, Z. Biomimetic design of reversibly unfolding cross-linker to enhance mechanical properties of 3D network polymers. *J. Am. Chem. Soc.* **129,** 14110–14111 (2007).
36. Burattini, S. *et al.* A healable supramolecular polymer blend based on aromatic π–π stacking and hydrogen-bonding interactions. *J. Am. Chem. Soc.* **132,** 12051–12058 (2010).
37. Kakuta, T. *et al.* Preorganized hydrogel: self-healing properties of supramolecular hydrogels formed by polymerization of host–guest-monomers that contain cyclodextrins and hydrophobic guest groups. *Adv. Mater.* **25,** 2849–2853 (2013).
38. Mozhdehi, D., Ayala, S., Cromwell, O. R. & Guan, Z. Self-healing multiphase polymers via dynamic metal–ligand interactions. *J. Am. Chem. Soc.* **136,** 16128–16131 (2014).
39. Pelrine, R., Kornbluh, R., Pei, Q. & Joseph, J. High-speed electrically actuated elastomers with strain greater than 100%. *Science* **287,** 836–839 (2000).
40. Anderson, I. A., Gisby, T. A., McKay, T. G., O'Brien, B. M. & Calius, E. P. Multi-functional dielectric elastomer artificial muscles for soft and smart machines. *J. Appl. Phys.* **112,** 041101 (2012).
41. Keplinger, C. *et al.* Stretchable, transparent, ionic conductors. *Science* **341,** 984–987 (2013).
42. Xie, T. Tunable polymer multi-shape memory effect. *Nature* **464,** 267–270 (2010).
43. Keplinger, C., Li, T., Baumgartner, R., Suo, Z. & Bauer, S. Harnessing snap-through instability in soft dielectrics to achieve giant voltage-triggered deformation. *Soft Matter* **8,** 285–288 (2012).
44. Hunt, S., McKay, T. G. & Anderson, I. A. A self-healing dielectric elastomer actuator. *Appl. Phys. Lett.* **104,** 113701 (2014).
45. Yuan, W. *et al.* Fault-tolerant dielectric elastomer actuators using single-walled carbon nanotube electrodes. *Adv. Mater.* **20,** 621–625 (2008).

Acknowledgements

This work was partially supported by the Major State Basic Research Development Program (Grant No. 2013CB922100 and Grant No. 2011CB808704), Air Force Office of Scientific Research (FA9550-15-1-0106) and Samsung Electronics. F.L. thanks the Swiss National Science Foundation for an Early Mobility Postdoc grant. We thank J. Ma for helpful discussions on the DFT calculations and X. R. Lu, J. C. Lai, X. Y. Jia and J. F. Mei for assistance in the synthesis and characterization of the model complex.

Author contributions

C.-H.L., C.W. and Z.B. conceived, designed and directed the project; C.-H.L., C.W., C.K., Y.S., P.Z., Y.C. and F.L. performed the experiments; C.-H.L., C.W., C.K., Y.S., P.Z., Y.C., F.L., J.-L.Z, X.-Z.Y., L.J., C.L. and Z.B. analysed the data; C.-H.L., C.W. and Z.B. wrote the paper. All the authors discussed the results and commented on the manuscript.

Additional information

Supplementary information is available in the online version of the paper. Reprints and permissions information is available online at www.nature.com/reprints. Correspondence and requests for materials should be addressed to Z.B.

Competing financial interests

Stanford University has filed a provisional application for a patent based on this technology that names C.H.L., C.W. and Z.B. as inventors.

© 2016 Macmillan Publishers Limited. All rights reserved